Title
Rare-Earth Disilicate-Silicon Nitride Ceramics: III. Strength and Creep Behavior

Authors
Cinibulk, M.K.
Thomas, G.
Johnson, S.M.

Publication Date
1991-11-01

LBL-31455
Preprint

Lawrence Berkeley Laboratory
UNIVERSITY OF CALIFORNIA

Materials & Chemical Sciences Division

Submitted to the Journal of the American Ceramic Society

Rare-Earth Disilicate–Silicon Nitride Ceramics: III. Strength and Creep Behavior

M.K. Cinibulk, G. Thomas, and S.M. Johnson

November 1991

Prepared for the U.S. Department of Energy under Contract Number DE-AC03-76SF00098

DISCLAIMER

LBL-31455

Rare-Earth Disilicate–Silicon Nitride Ceramics: III. Strength and Creep Behavior

Michael K. Cinibulk[#*] and Gareth Thomas[#]

Department of Materials Science and Mineral Engineering
University of California
and
Center for Advanced Materials
Materials Sciences Division
Lawrence Berkeley Laboratory
University of California
Berkeley, California 94720

Sylvia M. Johnson[#]

Materials Research Laboratory
SRI International
Menlo Park, CA 94025

November 1991

[#]Member, American Ceramic Society
[*]Currently with Max-Planck-Institut für Metallforschung, Stuttgart, FRG

This work was supported in part by the National Science Foundation under Contract No. DMR 83-1317239 and by the Director, Office of Energy Research, Office of Basic Energy Sciences, Materials Sciences Division, of the U.S. Department of Energy under Contract No. DE-AC03-76SF00098.

Abstract

The flexural strength and creep behavior of $RE_2Si_2O_7$-Si_3N_4 materials were examined. The retention in room-temperature strengths displayed by these ceramics at 1300°C was 80-91%, with no evidence of inelastic deformation preceding failure. The steady-state creep rates, at 1400°C in flexural mode, displayed by the most refractory materials are among the lowest reported for sintered Si_3N_4. The creep behavior was found to be strongly dependent on residual amorphous phase viscosity as well as on the oxidation behavior of these materials. All of the rare-earth oxide sintered materials, with the exception of $Sm_2Si_2O_7$-Si_3N_4, had lower creep strains than the $Y_2Si_2O_7$-Si_3N_4 material.
[Key Words: creep, microstructure, rare-earth oxides, silicon nitride, strength.]

I. Introduction

High-temperature mechanical behavior is adversely affected by an amorphous intergranular phase present in all sintered silicon nitride ceramics. Processing to obtain high density Si_3N_4 requires the use of sintering aids to provide a medium for liquid-phase sintering. These sintering aids react with the everpresent oxide layer on the surface of Si_3N_4 particles to form a eutectic liquid phase in which solution-reprecipitation of the Si_3N_4 particles occurs. It is the resulting amorphous phase that can soften at elevated temperatures, leading to subcritical growth of inherent flaws in the material due to stress-enhanced grain-boundary sliding and cavitation at the crack tip. The rate of grain-boundary sliding at a given temperature is inversely related to the viscosity of the amorphous grain-boundary phase. The presence of impurities is also known to degrade both room-temperature strength by the formation of inclusions resulting in stress-concentrations, and high-temperature properties by reducing the viscosity of the intergranular amorphous phase. Recent efforts in improving the high-temperature strength have been concerned with crystallizing the intergranular phase.[1-6]

The heavier lanthanide oxides (oxides of Sm→Yb), having high melting points and behaving similarly to Y_2O_3, have received limited attention as sintering additives[7], and their effect on high-temperature strength and creep behavior has not been reported. A few studies[8,9] have discussed the high-temperature strength of Si_3N_4 sintered with the lighter lanthanide oxides (oxides of La, Ce, Nd, or Sm), and found that these materials had slightly lower strengths at room-temperature and slightly higher strengths at 1370°C, than the Y-sintered material.[9]

The design, fabrication, and microstructural characterization of RE_2O_3-sintered Si_3N_4 ceramics tailored specifically for high temperatures has been previously described.[10] The lanthanide oxides have been found to be as effective as Y_2O_3 in densifying Si_3N_4, resulting in identical microstructures with densities of 98-99% of theoretical density. Complete crystallization of the intergranular phase was obtained with the exception of a thin residual amorphous film which was observed at interfaces and believed to be where impurities segregated, resulting in incomplete devitrification. In this paper the strength and creep resistance of Si_3N_4 sintered with rare-earth oxide additives tailored to obtain a $RE_2Si_2O_7$ secondary phase is detailed.

II. Experimental Procedure

(1) Material

The sintered Si_3N_4† ceramics were prepared with a 2:1 molar ratio of SiO_2:RE_2O_3, placing the composition directly on the Si_3N_4-$RE_2Si_2O_7$ tie line.[10] These materials contain a 12.3 vol% grain-boundary phase; this volume fraction is equivalent to a 15 wt% $Y_2Si_2O_7$-Si_3N_4 material. The materials were subjected to a heat-treatment at 1400°C for 24 hr to crystallize the secondary $RE_2Si_2O_7$ phase. X-ray diffraction and electron microscopy confirmed a completely crystalline secondary phase with a thin (on the order of 10 nm) residual amorphous film at all two-grain boundaries for all materials with the exception of

the $Yb_2Si_2O_7$-Si_3N_4 material. The $Yb_2Si_2O_7$-Si_3N_4 material had isolated regions with incompletely devitrified multiple-grain junctions, which were attributable to compositional heterogeneities in the powder compact during processing.

(2) Flexural Strength

Flexural strength tests were conducted at room temperature and at 1300°C. Four-point flexure testing was conducted in accordance with standards and specifications set by the U.S. Army Materials Technology Laboratory.[11] Test specimens 3 mm x 4 mm x 45 mm were cut and machined from the sintered samples. The specimens were tested as-ground (using a 320 grit diamond wheel) with edges chamfered to eliminate machining flaws that could act as initiation sites for fracture. The four-point test fixture consisted of a 40 mm outer support span and a 20 mm inner load span. Tests were conducted in laboratory air with a cross-head speed of 0.5 mm/min using a universal testing instrument. At 1300°C a modified high-temperature box furnace was placed between the frame of the testing instrument. The specimens entered the furnace at ~500°C and were heated to 1300°C in 15 min. The system was then allowed to thermally equilibrate for an additional 15 min prior to loading A minimum of six specimens were tested to obtain a single datum.

(3) Creep Behavior

Creep testing was carried out at 1400°C in four-point bending mode, adopting the specifications used for fast fracture tests. The test fixture and furnace used for flexural strength testing were also used for creep testing. Static loads ranging from 30 MPa to 170 MPa were applied to the specimen and the load-point displacement continuously measured by an external linear variable differential transducer (LVDT). This displacement was plotted on a strip-chart recorder as a function of time. The method of Hollenberg et al.[12] was used to analyze the data to determine maximum outer fiber stresses and strains.

(4) Microstructural Characterization

The fracture surface of the flexural strength specimens were characterized by scanning electron microscopy and energy-dispersive x-ray spectroscopy. Evidence of

deformation mechanisms of the Si_3N_4 materials that underwent creep were examined in a transmission electron microscope operated at 120 kV and equipped with an energy-dispersive x-ray spectrometer incorporating an ultra-thin window detector for analysis of elements with atomic number ≥5. Specimens for TEM were prepared by ion beam thinning to achieve electron transparency. A thin layer of carbon was evaporated onto both SEM and TEM specimens to minimize charging under the electron beam.

III. Results

(1) Flexural Strength

Flexural strengths at room temperature and at 1300°C are plotted versus temperature in Fig. 1. Room-temperature strengths were generally found to be dependent on porosity levels present in the ceramics. The $Sm_2Si_2O_7$-Si_3N_4 material, with the lowest density of all materials at 98.0%, had the lowest average strength of 533 MPa while the $Yb_2Si_2O_7$-Si_3N_4 material with one of the highest densities at 99.6% had the highest average strength of 623 MPa. Strengths as high as ~740 MPa were obtained for both the $Gd_2Si_2O_7$-Si_3N_4 and $Yb_2Si_2O_7$-Si_3N_4 materials at room-temperature. The values for the Weibull moduli ranged from a low of 6 for the $Er_2Si_2O_7$-Si_3N_4 strength data material to a high of 15 for the $Dy_2Si_2O_7$-Si_3N_4 strength data material (summarized in Table I).

For the flexural strengths obtained at 1300°C the same general trend of strength dependence on porosity level continued with a few exceptions, indicating additional failure mechanisms were operating at this temperature. Analysis of the load vs. deflection curve produced by the chart recorder revealed linear elastic behavior from the onset of loading to failure. No load relaxation occurred during these tests, which would have been indicative of fracture by slow crack growth, and would have been accompanied by a rapid decrease in strength.[13,14]

Although its room-temperature strength (and density) was the lowest among the materials tested, the $Sm_2Si_2O_7$-Si_3N_4 material had the highest average strength of 585 MPa

at 1300°C, ~10% higher than its own room-temperature strength. All other materials displayed a loss in strength at 1300°C of between 9% for the $Er_2Si_2O_7$-Si_3N_4 and $Yb_2Si_2O_7$-Si_3N_4 materials, to 20% for the $Gd_2Si_2O_7$-Si_3N_4 material. At 1300°C, the $Yb_2Si_2O_7$-Si_3N_4 material had an average strength of 567 MPa, while the lowest average strength of 467 MPa was displayed by the $Dy_2Si_2O_7$-Si_3N_4 material. Weibull moduli of these strength data ranged from a low of 14 for the $Yb_2Si_2O_7$-Si_3N_4 material to a high of 43 for the $Sm_2Si_2O_7$-Si_3N_4 material, shown in Table I. These moduli, which are much higher than those obtained from the room-temperature data, indicate both the reduced dependence of failure from flaws present in these materials, as well as the effect of increased crack blunting due to plastic deformation by the softening of the thin residual amorphous film at elevated temperatures.[15,16] It should be noted that the statistical validity of these moduli is likely to be low since they were calculated from a small data set and therefore they should only be used as preliminary values.

Based on the much lower strength of the $Sm_2Si_2O_7$-Si_3N_4 material at low temperatures and its high surface porosity, healing of surface flaws through crack blunting by oxidation of the surface occuring during the brief 15 min exposure at 1300°C prior to testing may be responsible for the increased strength at the elevated temperature.[17,18] This composition exhibited the greatest weight gain during oxidation[19] and it would be expected as well that flaw healing would have the greatest effect on minimizing crack initiation from surface porosity in this material.

Strength limiting flaws of those materials tested at room-temperature were common processing defects such as pores, powder agglomerates, and inclusions, located either at the tensile surface or just below it. Inclusions commonly found in the form of spherical particles were composed of primarily Si, Fe, and Ti, while other particles of similar morphology were composed of primarily Si, Al, and Ca, shown in Fig. 2 Other common types of inclusions appeared to be in the form of platelets (Fig. 2) and were identified by EDS to be composed primarily of Si with some minor amounts of the appropriate rare-earth

element. These latter inclusions are assumed to be SiO_2-rich glasses or devitrification products resulting from inadequate mixing of the sintering additives during processing.

At 1300°C strength limiting flaws were observed to be similar to those found in materials tested at room temperature. Some fracture surfaces displayed flaws that were large inclusions of what appear to be a glassy phase or its devitrification product (Fig. 2), attributed to incomplete powder homogenization during processing. At the fracture surfaces of the materials tested at 1300°C the glassy inclusions seem to have softened during the flexure test. Again, the composition of the glass was primarily Si, with a trace amount of RE.

(3) Creep

(1) Creep Behavior: The creep strain vs. time curves consisted of two characteristic regions for times up to 100 hr. In this study no true steady-state stage was encountered, instead a continuously decreasing creep rate was observed. This behavior has been reported in the literature for Si_3N_4 ceramics tested in uniaxial tension,[20-22] uniaxial compression,[22,23] and in four-point bending,[22,24,25] and has been attributed to the effects of oxidation and also to further crystallization of the grain-boundary phase occuring continuously during testing. Both processes lead to an increase in creep resistance; during oxidation, impurities migrate along and eventually out of the amorphous intergranular phase as they reach the bulk surface oxide interface, The net effect is a continuous increase in viscosity of the residual amorphous phase and even subsequent devitrification of the destabilized glass. Only for those samples that failed during testing was there evidence of the tertiary stage of creep behavior, characterized by a rapidly increasing rate of strain, lasting only 2-4 hr.

Because of the lack of a true steady-state regime all tests were allowed to proceed for 70 hr, since by this time the slope of the curve had decreased to a point approaching a near steady state. The slope was then obtained from the previous 8-10 hr. Longer times would have given lower "steady-state" creep rates, however extended test periods would

have been impractical due to test fixture geometry and experimental logistics. The typical length of time for creep studies of Si_3N_4 in the literature varies anywhere from 20 hr to over 150 hr.

A plot of "steady-state" creep rate as a function of applied load at 1400°C is shown in Fig. 3. It is evident that the creep deformation behavior of all these materials is similar. The strain rates are all within an order of magnitude and the slopes of the lines fitting the data are very similar as well. The slopes, being equal to the creep stress exponent, were determined to be in the range of 1.6 to 2.0. Values for n within this range have been reported for Si_3N_4 ceramics similarly tested and are expected when cavitation-induced creep is the dominant deformation mechanism.

The $Dy_2Si_2O_7$-Si_3N_4 and $Gd_2Si_2O_7$-Si_3N_4 materials displayed a surprisingly high resistance to creep based on their lower retention of fast-fracture strength at 1300°C, relative to the other materials. The $Sm_2Si_2O_7$-Si_3N_4 material displayed the poorest resistance to creep, while displaying the highest fast-fracture strength at 1300°C. The creep behavior results also indicate that with the exception of the $Sm_2Si_2O_7$-Si_3N_4 material, all materials displayed better resistance to creep than the $Y_2Si_2O_7$-Si_3N_4 ceramic. For applied loads of ~100 MPa creep rates ranged from about 2.0×10^{-5} to 1.3×10^{-4} hr^{-1}.

(2) Microstructures Following Creep: Selected materials were chosen to be examined after undergoing creep, using transmission electron microscopy, for evidence of cavity nucleation, growth, and coalescence leading to microcrack formation, commonly reported as the rate-determining deformation mechanism in liquid-phase sintered ceramics. Specimens were prepared such that the electron transparent regions were within 1 mm of the tensile surface of the test specimen.

Rather than being homogeneously distributed throughout the material, distinct clusters of cavities along with occasional isolated cavities were most often observed. The $Sm_2Si_2O_7$-Si_3N_4 material contained the greatest concentration of cavities of the three materials examined, while the $Dy_2Si_2O_7$-Si_3N_4 material had the lowest. With the exception

of the concentration of cavities, the cavitation of all three materials was very similar. Small cavities were found almost exclusively at multiple-grain junctions, with only a few observed at two-grain interfaces. Fig. 4 shows the nucleation of a cavity at a triple-grain junction. A common feature of the fully grown cavities was the presence of a thin film of amorphous material continuously coating the perimeter. Fig. 4 also shows the residual amorphous film lining a cavity following growth. EDS analysis of the residual amorphous film indicated the presence of little Dy or other impurities in this $Dy_2Si_2O_7$-Si_3N_4 specimen, indicating the depletion of cations in the residual amorphous phase due to cation migration to the oxidized surface during testing. The presence of these amorphous films could also be attributed to damage during ion-milling, as discussed by other investigators.[23,26] Since all multiple-grain junctions were found to have crystallized completely following heat treating (with the exception of a small fraction in the $Yb_2Si_2O_7$-Si_3N_4 material), it is believed that cavity nucleation occurred at the interface of β-Si_3N_4 and disilicate grains where a thin amorphous film exists. Growth of these cavities probably proceeds, following the viscous flow of the vitreous phase, by a diffusive growth mechanism resulting in a loss of the disilicate phase or possibly β-Si_3N_4.[27,28]

Evidence of grain-boundary sliding in the form of "strain whorls" was observed at a few two-grain boundaries. Such "strain whorls" have been previously reported[27,29] in materials examined after creep. The whorls have been described by Lange at al.[30] as extinction contours resulting from a localized out-of-plane buckling of the specimen. The extinction contours are an indication of contact stresses between the grains.

IV. Discussion

(1) Strength

The microstructures of all materials fabricated in this study were essentially identical with respect to grain size and morphology and crystalline nature of the secondary phase. Room-temperature strengths were directly related to the density of these materials. At the

elevated temperature all materials with the exception of the $Sm_2Si_2O_7$-Si_3N_4 material showed a decrease in strength of 9-20%. The high-temperature strengths followed the same relation to density as those at room-temperature, with a lack of nonlinear deformation preceding fracture indicative of the refractoriness of these materials. The retentions in strength of these materials could be roughly correlated with the RE_2O_3-SiO_2 binary eutectic temperatures, giving a relative approximation of the refractoriness of the residual amorphous phases present in each material. The strength at 1300°C, however, is as much dependent on flaws present in these materials as on the refractoriness of the grain-boundary phases. This point is exemplified in the behavior of the $Sm_2Si_2O_7$-Si_3N_4 material at the elevated temperature. The results of oxidation[10] and creep tests suggest that the refractoriness of the $Sm_2Si_2O_7$-Si_3N_4 material is somewhat less than that of the other five materials. However, the strength obtained at 1300°C of the $Sm_2Si_2O_7$-Si_3N_4 material was the highest, 10% higher than its room-temperature strength which was the lowest of all materials tested. The low room-temperature strength is believed to be due to the low bulk density and therefore high flaw population in this material. An increase in strength at 1300°C seems to indicate a healing of surface flaws during the 15 min exposure during testing by crack tip blunting, thereby reducing stress concentrations.[17,18]

Some plastically induced fracture resistance was observed at 1300°C based on the much higher Weibull modulii of the high-temperature strength data than those obtained of the room-temperature data, indicating the effect of increased crack blunting due to plastic deformation by the softening of the thin residual amorphous film at elevated temperatures. However, softening of the amorphous phase is not to the magnitude necessary for large-scale grain-boundary sliding and nonlinear deformation prior to failure.

(2) Creep Mechanism

In liquid-phase sintered ceramics, creep damage in the form of cavitation nucleation and growth at the multiple-grain junctions has been shown to dominate creep life.[20,23,26-28] The creep of Si_3N_4 ceramics containing an amorphous intergranular phase has been

shown to proceed by a combination of diffusional creep and cavitational creep.[23,26] Diffusional creep is presumed to occur by the redistribution of matter through the viscous grain-boundary phase. Dissolution of Si_3N_4 into the viscous phase and subsequent reprecipitation is driven by differential chemical potentials that arise from localized stresses.[23] Cavitational creep relies on grain-boundary sliding for the nucleation and growth of cavities to occur.[30]

In Si_3N_4 materials with crystalline grain-boundary phases, cavitational creep proceeds by a combination of cavity nucleation at the thin residual amorphous phase followed by diffusive cavitation growth at the expense of the secondary phase.[27,28] The thin residual amorphous film means that these sites are extremely small and therefore the cavity density of these materials has been shown to be much less than that of materials containing a completely amorphous secondary phase.[28] Subsequent stages of failure are then expected to involve the coalescence of cavities to form discrete microcracks.

Observations of cavitation nucleation and growth in the present study indicate the nucleation of grains occuring at multiple-grain junctions at the interface of Si_3N_4-Si_3N_4 grains and the interface of Si_3N_4-$RE_2Si_2O_7$ grains where the thin amorphous film exists. Following nucleation and depletion of the residual amorphous phase, growth proceeds by diffusion in the crystalline phases. Observations of cavity growth suggest that diffusional growth proceeds primarily at the expense of the rare-earth disilicates. The coalescence of cavities was observed, although the formation of microcracks from these cavities between the β-Si_3N_4 grains was rarely observed. The low strains exhibited by the materials examined by TEM may have been inadequate for the formation of a high density of microcracks since cavitation density was low.

(3) Oxidation Effects on Creep Behavior

The materials tested in creep in this study all displayed a continuing decrease in strain-rate with time. This behavior has been reported previously in the literature and has been attributed to both devitrification of the grain-boundary phase and oxidation effects

occuring throughout the duration of the test.[21,22,24,31] The present materials were all believed to have crystallized to the fullest extent, i.e., complete crystallization of the multiple-grain junctions with a thin residual amorphous film remaining at the two-grain boundaries. Therefore devitrification effects are not believed to be the main reason for the continued decrease in strain-rate. Oxidation of these materials, however, is thought to lead to an increase in the refractoriness of the ceramics by purifying the amorphous grain-boundary phase due to outward diffusion of impurity cations, thereby increasing its viscosity. As the concentration of glass-forming impurities decreases during oxidation the stability of the glass phase decreases as well, accelerating crystallization of this residual amorphous phase.[24]

The apparent conflicting results of the high-temperature strength tests and those of creep may be explained on the basis of the differences in defects present in the various materials and the refractoriness of the residual amorphous phases before and after oxidation. Defects play a greater role in determining the high-temperature strength of these materials than in determining the creep behavior. However, the composition of the grain-boundary phase has a stronger effect on creep behavior than it does on strength, when the materials are as refractory as the $RE_2Si_2O_7$-Si_3N_4 ceramics have shown to be. The relative retention in room-temperature strengths of these materials at 1300°C can be correlated with their oxidation resistances[19], with the notable exception of the behavior exhibited by the $Sm_2Si_2O_7$-Si_3N_4 material. Comparing the specific weight gains during oxidation of these materials with the "steady-state" creep strains, those materials having the highest weight gains had some of the highest creep strains. It is proposed that while the initial composition of the residual grain-boundary phase dictates high-temperature fast-fracture strength and oxidation resistance, the effect of oxidation on this phase during creep, which includes out-diffusion of impurity cations which increase the viscosity and accelerates subsequent devitrification must be considered when discussing the time-dependent behavior of these materials.

For example, $Yb_2Si_2O_7$-Si_3N_4 displayed among the highest strengths at both 25°C and 1300°C and a high strength in retention of 91%. However, its resistance to creep was found to be greater than only that of $Sm_2Si_2O_7$-Si_3N_4 and $Y_2Si_2O_7$-Si_3N_4. The specific weight gain after oxidation was the lowest after that of $Er_2Si_2O_7$-Si_3N_4. $Gd_2Si_2O_7$-Si_3N_4 also gave one of the highest room-temperature strengths, however, retained only 80% of that strength at 1300°C, the lowest of the six materials studied. Its resistance to creep was the greatest, next to that of $Dy_2Si_2O_7$-Si_3N_4, and it exhibited the greatest specific-weight gain during oxidation, excluding that of $Sm_2Si_2O_7$-Si_3N_4. The high oxidation rate of this material is believed to be responsible for the enhanced refractoriness of this material resulting from the out-diffusion of impurity cations, thereby creating a more refractory residual amorphous phase.

$Sm_2Si_2O_7$-Si_3N_4 had by a factor of two the greatest specific-weight gain upon oxidation of the six materials. The actual increase in strength at 1300°C was explained based on the relatively lower oxidation resistance of this material. The foregoing argument would lead to the reasoning that $Sm_2Si_2O_7$-Si_3N_4 should show the greatest resistance to creep of the six materials based on its rapid oxidation behavior and higher 1300°C strength. However, this material actually undergoes the greatest deformation in the group. The low refractoriness of the residual amorphous grain-boundary phase present in this material is believed to be so much lower than the refractoriness of the amorphous phases in the other materials that the effects of oxidation are insufficient to increase the refractoriness of this low-viscosity grain-boundary phase to that of the glass in the other five materials.

V. Conclusions

(1) The retention in room-temperature strength displayed by these ceramics at 1300°C is among the highest reported to date, with that of $Er_2Si_2O_7$-Si_3N_4 and $Yb_2Si_2O_7$-Si_3N_4 reaching 91%. $Sm_2Si_2O_7$-Si_3N_4 was found to increase in strength at the higher temperature by 10%. This has been attributed to surface flaw healing by oxidation of the

surface or blunting of internal flaws by softening of the g-b-phase occuring prior to testing. Fracture surfaces were found to contain metallic as well as nonmetallic inclusions. Failure initiation most often occurred at the tensile surface. There was no evidence of inelastic deformation preceding failure, indicative of the high refractoriness of these materials.

(2) The "steady-state" creep rates, at 1400°C in flexural mode, displayed by the most refractory materials are among the lowest reported. The creep behavior was found to be strongly dependent on residual amorphous phase viscosity as well as on the oxidation behavior of these materials, as evidenced by the nonsteady-state creep rates of all materials. As oxidation proceeds there is a purifying effect on the residual amorphous phases due to impurity diffusion to the surface. This purification results in higher viscosity glasses and destabilized glasses that may further devitrify. All of the rare-earth oxide sintered materials, with the exception of $Sm_2Si_2O_7$-Si_3N_4, had lower creep strains than the $Y_2Si_2O_7$-Si_3N_4 material.

(3) Examination of materials that were tested in creep indicates that deformation proceeds by grain-boundary cavitation. Cavities nucleate at the thin amorphous film between $RE_2Si_2O_7$-Si_3N_4 and Si_3N_4-Si_3N_4 grains. A diffusive mass transport mechanism results in cavity growth at the expense of $RE_2Si_2O_7$. Under the stresses applied to these materials at 1400°C, coalescence of cavities was frequently observed, but not, however to the degree necessary for microcrack formation.

Acknowledgments

We thank J. Porter, Rockwell International, for helpful discussions regarding creep testing and G. Craig, SRI International, for assistance with specimen preparation and mechanical testing.

† SN E-10, Ube Industries, Tokyo, Japan

Based on the dissertation submitted by M.K. Cinibulk for the Ph.D. degree in Materials Science and Engineering, University of California, Berkeley, CA 94720

Initially supported by the National Science Foundation under Contract No. DMR 83-1317239. Additional support was provided by the Director, Office of Energy Research, Office of Basic Energy Sciences, Materials Sciences Division of the U.S. Department of Energy under Contract No. DE-AC03-76SF00098. Additional facilities were provided by SRI International.

References

1. A. Tsuge, K. Nishida, and M. Komatsu, "Effect of Crystallizing the Grain-Boundary Phase on the High-Temperature Strength of Hot-Pressed Si_3N_4 Ceramics," J. Am. Ceram. Soc., **58** [7-8] 323-26 (1975).

2. J.E. Weston, P.L. Pratt, and B.C.H. Steele, "Crystallization of Grain-Boundary Phases in Hot-Pressed Silicon Nitride," J. Mater. Sci., **13** 2137-56 (1978).

3. D.R. Clarke, F.F. Lange, and G.D. Schnittgrund, "Strengthening of a Sintered Silicon Nitride by a Post-Fabrication Heat Treatment," J. Am. Ceram. Soc., **65** [4] C-51-52 (1982).

4. L.A. Pierce, D.M. Mieskowski, and W.A. Sanders, "Effect of Grain-Boundary Crystallization on the High-Temperature Strength of Silicon Nitride," J. Mater. Sci., **21** 1345-48 (1986).

5. D.A. Bonnell, T.-Y. Tien, and M. Rühle, "Controlled Crystallization of the Amorphous Phase in Silicon Nitride Ceramics, J. Am. Ceram. Soc., **70** [7] 460-65 (1987).

6. M.K. Cinibulk, G. Thomas, and S.M. Johnson, "Grain-Boundary-Phase Crystallization and Strength of Silicon Nitride Sintered with a YSiAlON Glass," J. Am. Ceram. Soc., **73** [6] 1606-12 (1990).

7. I.C. Huseby and G. Petzow, "Influence of Various Densifying Additives on Hot-Pressed Si_3N_4," Powder Metall. Int., **6** [1] 17-19 (1974).

8. F.F. Lange, "Si_3N_4-Ce_2O_3-SiO_2 Materials: Phase Relations and Strength," Am. Ceram. Soc. Bull., **59** [2] 239-40, 49 (1980).

9. W.A. Sanders and D.M. Mieskowski, "Strength and Microstructure of Sintered Si_3N_4 with Rare-Earth Oxide Additions," J. Am. Ceram. Soc., **64** [2] 304-09 (1985).

10. M.K. Cinibulk, G. Thomas, and S.M. Johnson, "$RE_2Si_2O_7$-Si_3N_4 Ceramics: I, Design, Fabrication, and Secondary-Phase Crystallization," J. Am. Ceram. Soc., this issue (1992).

11. MIL-STD-1942A, "Flexural Strength of High Performance Ceramics at Ambient Temperature," U.S. Army Materials Technology Laboratory, Watertown, MA, 1990.

12. G.W. Hollenberg, G.R. Terwilliger, and R.S. Gorden, "Calculation of Stresses and Strains in Four-Point Bending Creep Tests," J. Am. Ceram. Soc., **54** [4] 196-99 (1971).

13. N.J. Tighe, "The Structure of Slow Crack Interfaces in Silicon Nitride," J. Mater. Sci., **13** 1455-63 (1978).

14. J.T. Smith and C.L. Quackenbush, "Phase Effects in Si_3N_4 Containing Y_2O_3 or CeO_2: I, Strength," Am. Ceram. Soc. Bull., **59** [5] 529-32, 537 (1980).

15. R.K Govila, "Strength Characterization of Yttria-Doped Sintered Silicon Nitride," J. Mater. Sci., **20** 4345 (1985).

16. R.K. Govila, "Fracture Phenomenology of a Sintered Silicon Nitride Containing Oxide Additives," J. Mater. Sci., **23** 1141-50 (1988).

17. D.W. Richerson, Modern Ceramic Engineering, Marcel Dekker, Inc., New York, 1982.

18. L. Chuck, S.M. Goodrich, N.L. Hecht, and D.E. McCullum, "High-Temperature Tensile Strength and Stress Rupture Behavior of Norton/TRW NT-154 Silicon Nitride," Ceram. Eng. Sci. Proc., **11** [7-8] 1007-27 (1990).

19. M.K. Cinibulk, G. Thomas, and S.M. Johnson, "$RE_2Si_2O_7$-Si_3N_4 Ceramics: II, Oxidation Behavior," J. Am. Ceram. Soc., this issue (1992).

20. R. Kossowsky, D.G. Miller, and E.S. Diaz, "Tensile and Creep Strength of Hot-Pressed Si_3N_4," J. Mater. Sci., **10** 983-97 (1975).

21. R.M. Arons and J.K. Tien, "Creep and Strain Recovery in Hot-Pressed Silicon Nitride," J. Mater. Sci., **15** 2046-58 (1980).

22. M.K. Ferber, M.G. Jenkins, and V.J. Tennery, "Comparison of Tension, Compression, and Flexure Creep for Alumina and Silicon Nitride Ceramics," Ceram. Eng. Sci. Proc., **11** [7-8] 1028-45 (1990).

23. F.F. Lange, B.I. Davis, and D.R. Clarke, "Compressive Creep of Si_3N_4/MgO Alloys: Part 1, Effect of Composition," J. Mater. Sci., **15** 601-10 (1980).

24. B.S.B. Karunaratne and M.H. Lewis, "High-Temperature Fracture and Diffusional Deformation Mechanisms in Si-Al-O-N Ceramics," J. Mater. Sci., **15** 449-62 (1980).

25. S.M. Wiederhorn and N.J. Tighe, "Structural Reliability of Yttria-Doped Hot-Pressed Silicon Nitride at Elevated Temperatures," J. Am. Ceram. Soc., **66** [12] 884-89 (1983).

26. J.E. Marion, A.G. Evans, M.D. Drory, and D.R. Clarke, "High Temperature Failure Initiation in Liquid Phase Sintered Materials," Acta. Metall., **31** [10] 1445-57 (1983).

27. G.D. Quinn and W.R. Braue, "Secondary Phase Devitrification Effects upon the Static Fatigue Resistance of Sintered Silicon Nitride," Ceram. Eng. Sci. Proc., **11** [7-8] 616-32 (1990).

28. C.-F. Chen and T.-Y. Tien, "High Temperature Mechanical Properties of SiAlON Ceramics: Microstructural Effects," Ceram. Eng. Sci. Proc., **8** [7-8] 778-95 (1987).

29. F.F. Lange, D.R. Clarke, and B.I. Davis, "Compressive Creep of Si_3N_4/MgO Alloys, Part 2: Source of Viscoelastic Effect," J. Mater. Sci., **15** 611-15 (1980).

30. R.L. Tsai and R. Raj, "The Role of Grain-Boundary Sliding in Fracture of Hot-Pressed Si_3N_4 at High-Temperatures," J. Am. Ceram. Soc., **63** [9-10] 513-17 (1980).

31. F.F. Lange, B.I. Davis, and D.R. Clarke, "Compressive Creep of Si_3N_4/MgO Alloys: Part 3, Effects of Oxidation Induced Compositional Change," J. Mater. Sci., **15** 616-18 (1980).

Table I. Flexural Strength Results

Material	Strength* (MPa) 25°C/1300°C	Std. Dev. (MPa) 25°C/1300°C	Weibull Modulus 25°C/1300°C
$Y_2Si_2O_7$-Si_3N_4	599/523	69/37	10/17
$Sm_2Si_2O_7$-Si_3N_4	533/585	56/17	11/43
$Gd_2Si_2O_7$-Si_3N_4	615/490	68/26	10/23
$Dy_2Si_2O_7$-Si_3N_4	540/467	42/31	15/18
$Er_2Si_2O_7$-Si_3N_4	550/502	112/21	6/29
$Yb_2Si_2O_7$-Si_3N_4	623/567	93/49	8/14

* Mean strengths of six test specimens

Figure Captions

Figure 1. Plot of flexural strengths at 25°C and 1300°C. Error bars have been omitted for clarity. Standard deviations were ~10% and ~5% of mean strengths at 25°C and 1300°C, respectively.

Figure 2. Scanning electron micrographs of inclusions present on the fracture surfaces. (a) and (b) fractured at room temperature. (c) fractured at 1300°C.

Figure 3. Plot of "steady-state" creep strain rates as a function of applied stress at 1400°C. Creep stress exponents are given inset.

Figure 4. Transmission electron micrographs showing (a) cavity nucleation in $Y_2Si_2O_7$-Si_3N_4 and (b) residual amorphous phase surrounding perimeter of cavity in $Dy_2Si_2O_7$-Si_3N_4 material, imaged in dark-field.

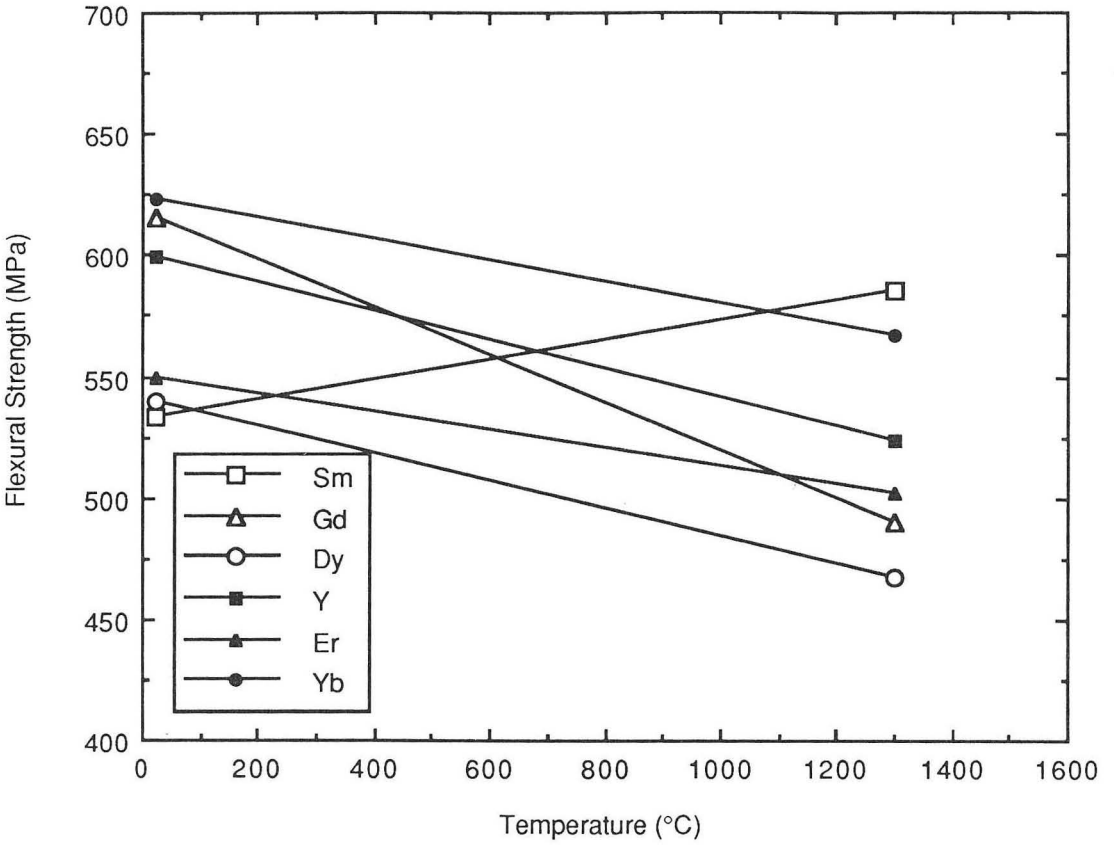

XBL 916-1288

Figure 1

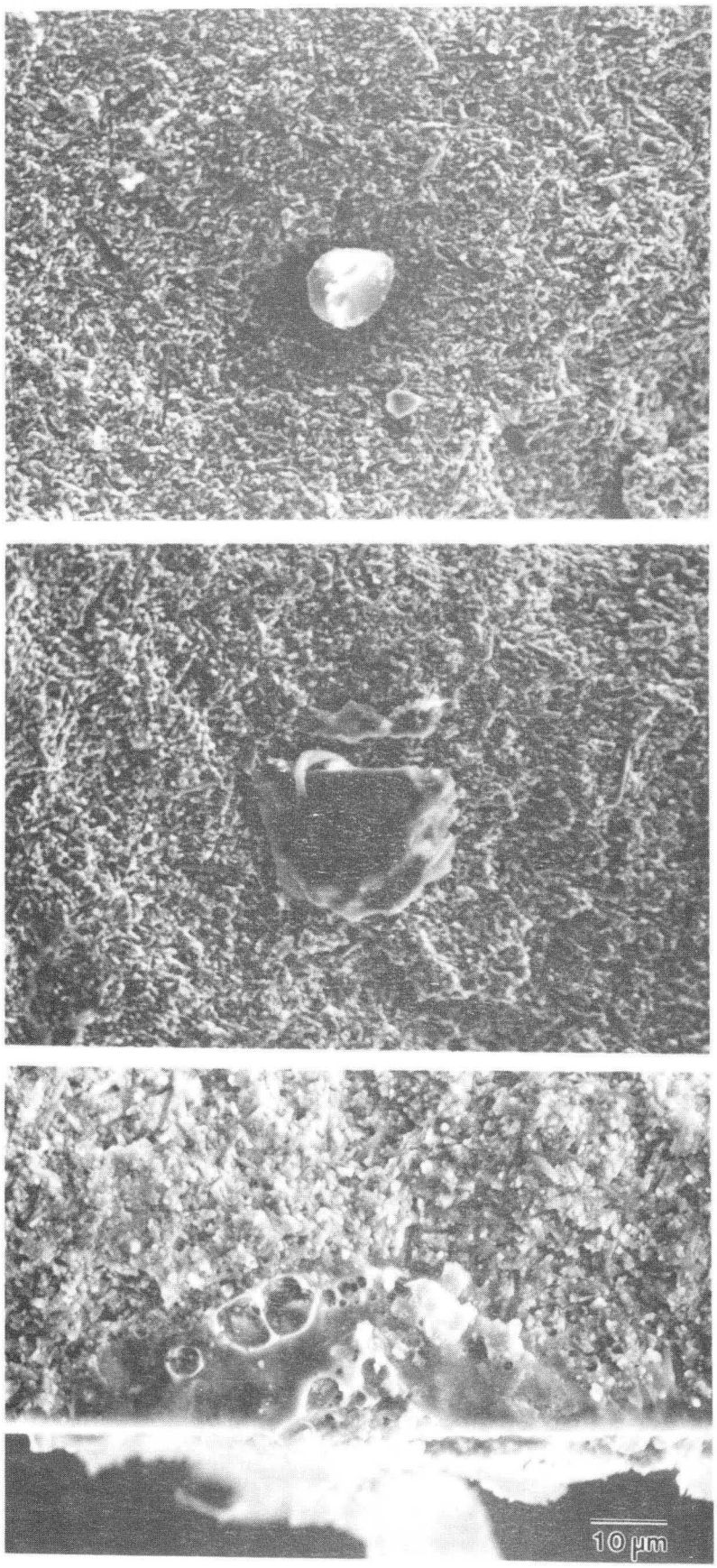

XBB 918-6291

Figure 2

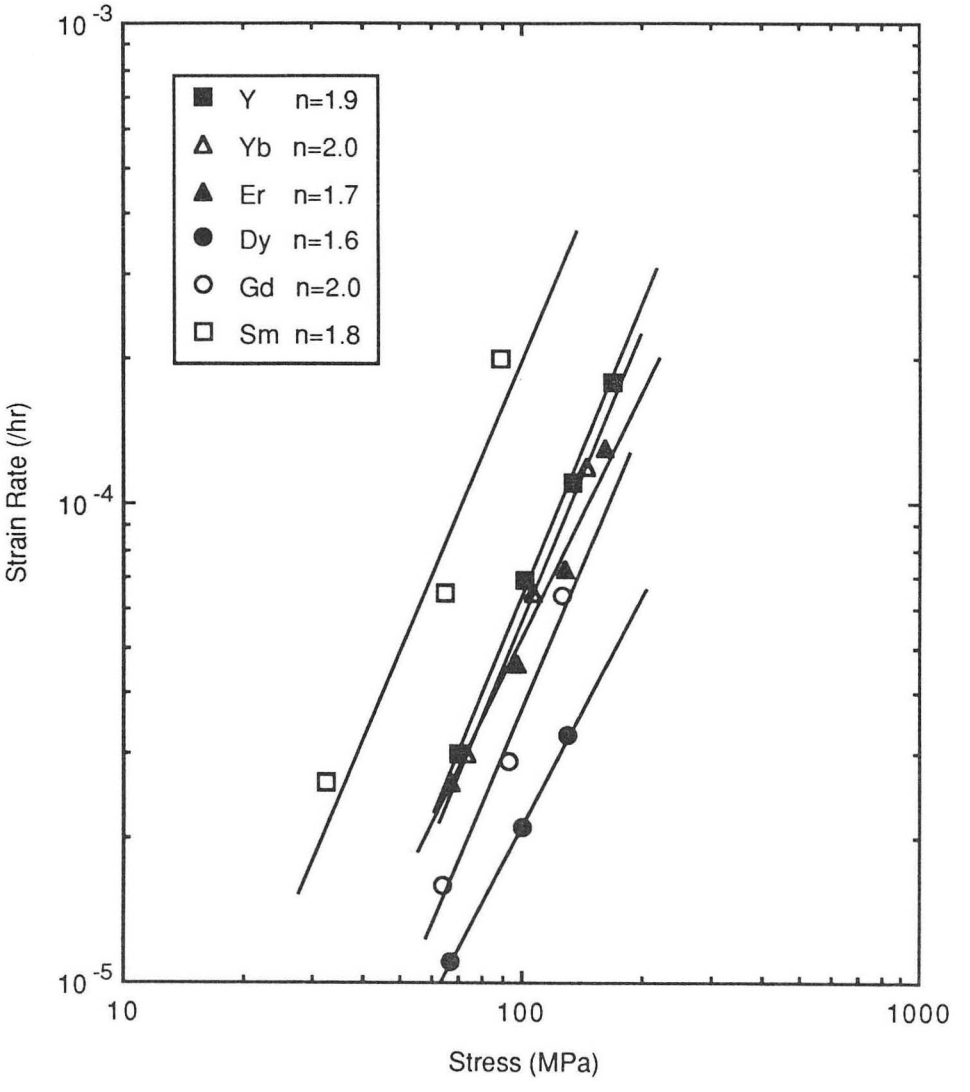
10 -3
10 -4
10 -5
Strain Rate (/hr)
10
100
1000
Stress (MPa)
Y n=1.9
Yb n=2.0
Er n=1.7
Dy n=1.6
Gd n=2.0
Sm n=1.8
XBL 916-1289

Figure 3

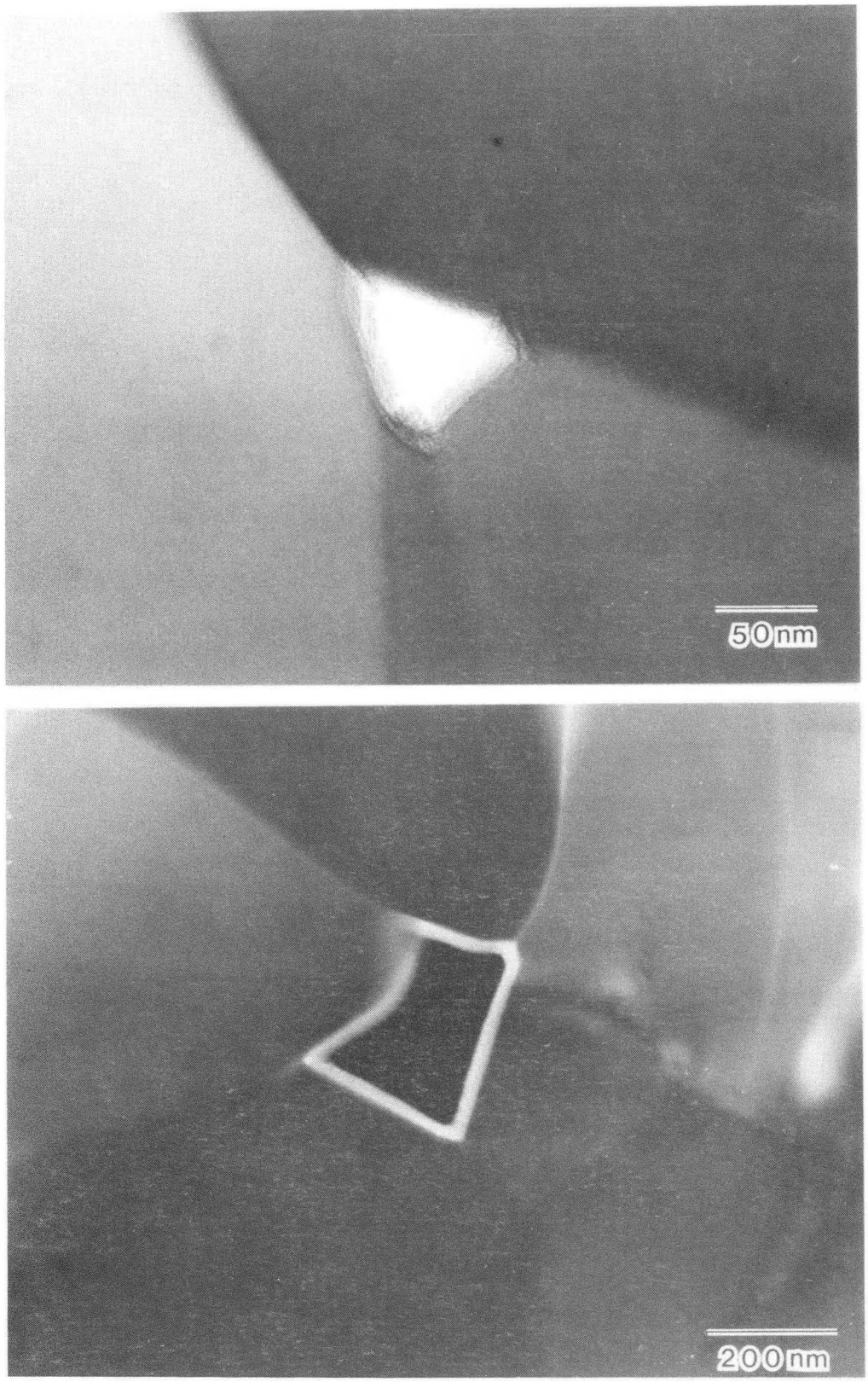

XBB 918-6290

Figure 4

LAWRENCE BERKELEY LABORATORY
UNIVERSITY OF CALIFORNIA
INFORMATION RESOURCES DEPARTMENT
BERKELEY, CALIFORNIA 94720